

# Inherent Speedup Limitations in Multiple Time Step/Particle Mesh Ewald Algorithms

DANNY BARASH, LINJING YANG, XIAOLIANG QIAN, TAMAR SCHLICK

*Department of Chemistry and Courant Institute of Mathematical Sciences, New York University  
and Howard Hughes Medical Institute, 251 Mercer Street, New York, New York 10012*

*Received 13 May 2002; Accepted 23 August 2002*

**Abstract:** Multiple time step (MTS) algorithms present an effective integration approach to reduce the computational cost of dynamics simulations. By using force splitting to allow larger time steps for the more slowly varying force components, computational savings can be realized. The Particle-Mesh-Ewald (PME) method has been independently devised to provide an effective and efficient treatment of the long-range electrostatics interactions. Here we examine the performance of a combined MTS/PME algorithm previously developed for AMBER on a large polymerase  $\beta$ /DNA complex containing 40,673 atoms. Our goal is to carefully combine the robust features of the Langevin/MTS (LN) methodology implemented in CHARMM—which uses position rather than velocity Verlet with stochasticity to make possible outer time steps of 150 fs—with the PME formulation. The developed MTS/PME integrator removes fast terms from the reciprocal-space Ewald component by using switch functions. We analyze the advantages and limitations of the resulting scheme by comparing performance to the single time step leapfrog Verlet integrator currently used in AMBER by evaluating different time-step protocols using three assessors for accuracy, speedup, and stability, all applied to long (i.e., nanosecond) simulations to ensure proper energy conservation. We also examine the performance of the algorithm on a parallel, distributed shared-memory computer (SGI Origin 2000 with 8 300-MHz R12000 processors). Good energy conservation and stability behavior can be demonstrated, for Newtonian protocols with outer time steps of up to 8 fs and Langevin protocols with outer time steps of up to 16 fs. Still, we emphasize the inherent limitations imposed by the incorporation of MTS methods into the PME formulation that may not be widely appreciated. Namely, the limiting factor on the largest outer time-step size, and hence speedup, is an intramolecular cancellation error inherent to PME. This error stems from the excluded-nonbonded correction term contained in the reciprocal-space component. This cancellation error varies in time and introduces artificial frequencies to the governing dynamics motion. Unfortunately, we find that this numerical PME error cannot be easily eliminated by refining the PME parameters (grid resolution and/or order of interpolating polynomial). We suggest that methods other than PME for fast electrostatics may allow users to reap the full advantages from MTS algorithms.

© 2002 Wiley Periodicals, Inc. J Comput Chem 24: 77–88, 2003

**Key words:** multiple time steps; particle-mesh Ewald; molecular dynamics; polymerase  $\beta$ ; AMBER program

## Introduction

Molecular dynamics (MD) simulations play an important role in elucidating essential functional properties in key biologic processes. Because of the crucial link between structure and function, structural information derived from experimental studies can be refined and interpreted at atomic resolution using all-atom computer simulations. The vision of the late Peter Kollman in introducing the AMBER force field,<sup>1</sup> among his many other important contributions, paved the way to numerous biomolecular discoveries both for protein and nucleic acid systems. Molecular modeling and simulation has already become a powerful vehicle for refining experimental models and for predicting in advance of experiment

new features that are of biologic importance (see the text<sup>2</sup> and references,<sup>3–17</sup> for example).

Modeling protein/DNA complexes using all-atom force fields presents a considerable challenge to the methodology, due to the

---

**Correspondence to:** T. Schlick; e-mail: schlick@nyu.edu

Contract/grant sponsor: NSF; contract/grant number: ASC-9318159

Contract/grant sponsor: NIH; contract/grant number: R01 GM55164

Contract/grant sponsor: National Computational Science Alliance; contract/grant number: MCA99S021N (NCSA SGI/CRAY Origin2000)

Contract/grant sponsor: John Simon Guggenheim fellowship to T. S. Computations

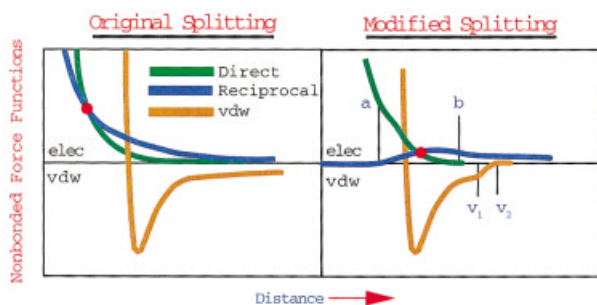


**Figure 1.** Force-splitting strategy for the MTS/PME algorithm. At left, forces are drawn before smooth switches are applied. The curve crossing indicates slow components in the direct term and fast components in the reciprocal term. After the switches are applied, the resulting splitting is shown at right. The Coulomb force is switched between distances  $a$  and  $b$ , whereas the van der Waals is switched between  $v_1$  and  $v_2$ .

heavy amount of computations involved in simulating long trajectories (several nanoseconds or more). The development of reliable and efficient methods for simulating biomolecules is thus an important but challenging task. Several efficient approaches have been suggested and examined for treating the expensive non-bonded computations; these include fast multipole,<sup>18</sup> PME,<sup>19</sup> and multigrid methods.<sup>20–22</sup> In tandem, multiple time step (MTS) methods<sup>23–26</sup> have been developed on the basis of splitting the forces into classes according to their range of interaction, thus enabling the update of the associated forces in an efficient manner. Here, we examine performance of a recent MTS/PME integrator implemented in AMBER<sup>27</sup> to uncover inherent limitations in MTS/PME algorithms. AMBER's PME integrator is based on the work of Darden and coworkers.<sup>28,29</sup> The MTS relies on ideas from Batcho et al.,<sup>30</sup> who adapted features of the LN algorithm in CHARMM,<sup>31</sup> and the update of Qian and Schlick,<sup>27</sup> who added switch functions to define the force classes. Switch functions have been used by Zhou et al.<sup>32</sup> and by Qian and Schlick,<sup>27</sup> because it had been shown that the reciprocal-space Ewald component contains fast terms and the direct-space Ewald component contains slow terms.<sup>32–34</sup> Smooth switch functions thus might push the fast terms to the direct-space component and slow terms into the reciprocal-space component, as shown in Figure 1.

Besides AMBER's protein benchmark system, we use a polymerase  $\beta$ /DNA complex,<sup>31</sup> which we simulated recently to identify the large-scale motions thought to be crucial for repair mechanisms during DNA synthesis and repair. The enzyme's function of filling in DNA gaps is thought to involve an "induced fit" mechanism, in which the enzyme alternates between open and closed states. The possible large-scale motion associated with the experimentally observed open and closed enzyme/DNA complex has been modeled using the CHARMM program (see ref. 35 for details). Here, we have ported the system to the AMBER program in the initial goal of producing an economical and reliable simulation protocol suitable for long trajectories. By applying the MTS/PME scheme to model the polymerase  $\beta$ /DNA system and comparing it with the single time step (STS) leapfrog Verlet integrator used in AMBER, we show that inherent speedup limitations emerge from the intramolecular PME cancellation error.

The need for a correction term arises because some near-neighbor nonbonded interactions are omitted from the Coulomb potential to avoid double counting these interactions in other terms of the potential. In practice, these excluded terms are subtracted from the Coulomb potential as evaluated by PME. While in the direct-space sum, these excluded Coulombic interactions are simply omitted, in the reciprocal-space term, they are calculated only to a finite degree of accuracy due to the cutoff in the reciprocal-space grid; thus, the subtraction of the excluded terms does not exactly cancel the implicitly-contained analog (in the reciprocal-space summation). This cancellation error varies in time, and introduces artificial frequencies to the governing dynamics motion.

Unfortunately, we find that this numerical PME error cannot be easily eliminated by refining the PME parameters (grid resolution and/or order of interpolating polynomial). Although we emphasize that the marriage between MTS and PME is questionable in terms of immediate practical gains, adapting successful MTS elements for an alternative long-range electrostatic treatment (e.g., refs. 21, 22, 36–38) and may be more fruitful.

The outline of this article is as follows. The next section describes the developed MTS/PME method. Ideas from the MTS/

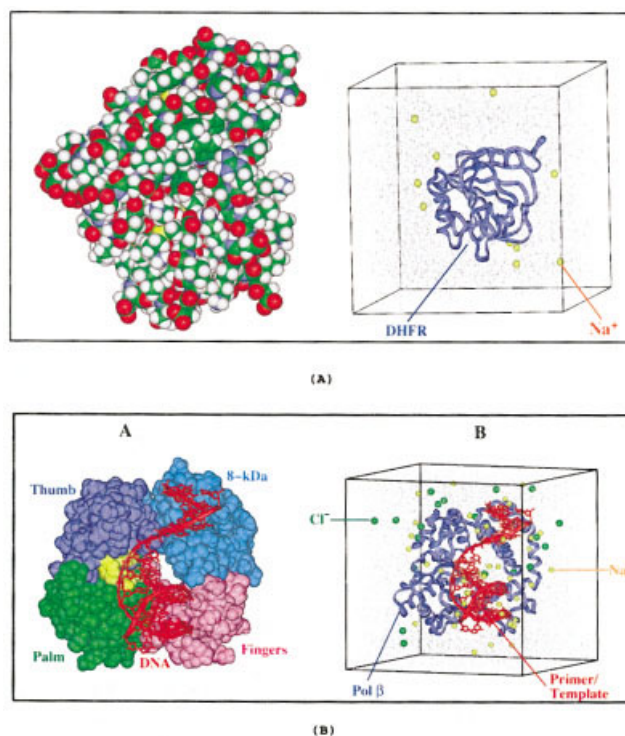


**Figure 2.** Biomolecular system. (A) The dihydrofolate reductase (DHFR) protein used as a benchmark to test the MTS/PME algorithm. The total solvated system size is 22,930 atoms (2489 protein atoms, 20,430 water molecules, and 11 ions). (B) The pol  $\beta$ /DNA complex used as a large-scale test system for our MTS/PME algorithm is shown at left; key protein residues in the active site are yellow, and DNA atoms are red. The enzyme's various domains are shown. At right, the solvated model of pol  $\beta$ /DNA complex in a cubic domain is illustrated. The system consists of 11,399 bulk water molecules (gray), 42  $\text{Na}^+$  (yellow), and 20  $\text{Cl}^-$  (green) counterions.

Langevin (LN) CHARMM implementation<sup>31</sup> motivate the force splitting strategy used in ref. 27. Expected advantages and limitations are also discussed. Then we report performance of the MTS/PME integrator on biomolecular systems with AMBER 6.0; performance is analyzed in terms of various accuracy (based on static or average quantities), stability (dynamic information), and speedup assessors. Parallelization issues are examined, as are the inherent speedup limitations in MTS/PME algorithms (stemming from an outer time-step limit to manage the intramolecular cancellation error for large systems).

## Method

### Overview

The Verlet/Störmer method,<sup>39,40</sup> with all its variants, is at the heart of most MD simulations due to its favorable numerical properties. Here we briefly sketch the main ideas, starting from the original Verlet algorithm, on which most force splitting strategies are based. We refer the interested reader to a general introduction on the subject,<sup>2</sup> and to an earlier article<sup>27</sup> for more details about the proposed MTS/PME algorithm.

In classical dynamics, the motion of a molecular system obeys Newton's classical equation of motion:

$$\mathbf{M}\ddot{X}(t) = F(X(t)) = -\nabla E(X(t)). \quad (1)$$

Here, the position vector  $X \in \mathbf{R}^{3N}$  denotes the coordinates of each atom;  $\mathbf{M}$  is the diagonal mass matrix, with the masses of each atom repeated three times along the diagonal. The dot superscripts denote differentiation with respect to time,  $t$ ,  $F$  is the total force, and  $E$  is the potential energy.

The Verlet algorithm uses the following discretization for the trajectory positions to advance in time:

$$X^{n+1} = 2X^n - X^{n-1} + \Delta t^2 F^n. \quad (2)$$

In the scheme above, superscripts  $n$  denote the finite-difference approximations to quantities at time step  $n\Delta t$ . Different Verlet variants have been devised, based on the flexibility in defining corresponding velocity propagation formulas consistent with eq. (2).

In an effort to reduce the computational cost when using the Verlet algorithm, an attractive idea is to use the multiple time step (MTS) algorithms mentioned earlier. Because the total force term  $F$  in eq. (1) reflects components varying in their ranges of interaction, efficiency in MD simulations can be achieved by splitting the force into several classes, for example fast, medium, and slow, and using different update frequencies for them. Thus, the force components  $F_{\text{fast}}$ ,  $F_{\text{med}}$ ,  $F_{\text{slow}}$  are associated with corresponding time steps  $\Delta\tau$ ,  $\Delta t_m$ , and  $\Delta t$ , where the integers  $k_1$  and  $k_2$  relate the time steps by

$$k_1 = \Delta t_m / \Delta\tau, \quad k_2 = \Delta t / \Delta t_m. \quad (3)$$

We also introduce the ratio  $r$ :

$$r = k_1 k_2 = \Delta t / \Delta\tau, \quad (4)$$

between the outer and inner time step. This ratio provides an upper limit on overall speedup.

In the context of PME, the challenge is to define the medium and slow classes because the direct PME has slow components while the reciprocal PME component has fast terms.<sup>27</sup> We discuss this crucial point in the next section.

Recent work on the LN algorithm in CHARMM (see earlier, and the general ref. 2 for more details) has shown that force splitting by extrapolation rather than impulses<sup>41,42</sup> and the use of position rather than velocity Verlet<sup>43,44</sup> are advantageous in terms of stability and accuracy. In addition, the introduction of stochasticity by using Langevin dynamics rather than Newtonian dynamics<sup>41</sup> alleviates severe resonance effects and results in better numerical behavior. The Langevin equation extends eq. (1) and is given by:

$$\mathbf{M}\ddot{X}(t) = -\nabla E(X(t)) - \gamma\mathbf{M}\dot{X}(t) + R(t), \quad (5)$$

where  $\gamma$  is the collision parameter, or damping constant. The random-force vector  $R$  is a stationary Gaussian process with statistical properties given by:

$$\langle R(t) \rangle = 0, \quad \langle R(t) R(t')^T \rangle = 2\gamma k_B T \mathbf{M} \delta(t - t'), \quad (6)$$

where  $k_B$  is the Boltzmann constant,  $T$  is the target temperature, and  $\delta$  is the Dirac symbol for the delta function.

The LN method can be sketched as follows for a three-class force-splitting scheme:

### LN Algorithm

```

 $X_r^0 \equiv X$ 
 $F_{\text{slow}} \equiv -\nabla E_{\text{slow}}(X_r)$ 
For  $j = 1$  to  $k_2$ 
   $X_r \equiv X_r^j \leftarrow X + \frac{\Delta t_m}{2} V$ 
   $F_{\text{med}} = -\nabla E_{\text{med}}(X_r)$ 
   $F \leftarrow F_{\text{med}} + F_{\text{slow}}$ 
  For  $i = 1$  to  $k_1$ 
     $X \leftarrow X + \frac{\Delta\tau}{2} V$ 
     $V \leftarrow (V + \mathbf{M}^{-1} \Delta\tau (F + F_{\text{fast}}(X) + R)) / (1 + \gamma \Delta\tau)$ 
     $X \leftarrow X + \frac{\Delta\tau}{2} V$ 
  End
End

```

Note here the use of extrapolation (a slow-force contribution is made each time the fast force is evaluated in the inner loop, i.e., every  $\Delta\tau$  interval), position Verlet in the inner loop, and Langevin dynamics (random and frictional terms). The Gaussian random force  $R$  is chosen each inner time step by a standard procedure (e.g., Box/Muller method<sup>45</sup>) according to the target temperature. In the next subsection, we describe an extension of the LN algorithm above tailored for PME algorithms.

### Force-Splitting Considerations

In PME methods, the Coulomb force is summed from a direct term, a reciprocal term, and correction terms (see Appendix for the exact expressions of each term):

$$F_c = F_{\text{direct}} + F_{\text{reciprocal}} + F_{\text{cor,self}} + F_{\text{cor,ex}} + F_{\text{cor,e}} \quad (8)$$

As noted by Stuart et al.,<sup>34</sup> Batcho et al.,<sup>30</sup> Zhou et al.,<sup>32</sup>, and Qian and Schlick,<sup>27</sup> the direct term has a “tail” (slow terms), whereas the reciprocal term has a “head” (fast terms). This behavior, illustrated in Figure 1, means that simply assigning the reciprocal term into the slow class and the direct term into the medium class limits the time step that can be used in an MTS/PME algorithm. Indeed, compared to the outer time step  $\Delta t = 150$  fs used in the Langevin/MTS protocol in CHARMM, the AMBER MTS/PME protocols discussed here show limits of  $\Delta t = 6$  fs and 16 fs for Newtonian and Langevin dynamics, respectively. Thus, the idea of using switch functions<sup>27,32</sup> appears attractive. Besides possibly allowing large time steps, a separate smooth switch function on the van der Waals force results in an improved representation over force-splitting methods applied to truncated van der Waals terms, as in Batcho et al.<sup>30</sup>

We thus use a three-level force-splitting strategy that assigns switched forces into the different classes (see Fig. 1 for illustration):

$$\begin{aligned} F_{\text{fast}} &= F_{\text{bond}} + F_{\text{angle}} + F_{\text{torsion}} \\ F_{\text{med}} &= F_{\text{direct}}^{\text{switched}} + F_{\text{vdw}}^{\text{switched}}, \\ F_{\text{slow}} &= F_{\text{reciprocal}}^{\text{switched}} \end{aligned}$$

where expressions for the various terms can be found in the Appendix.

Thus, the switched direct-space and switched van der Waals forces are assigned to the medium class, and the switched reciprocal-space forces are assigned to the slow class. In addition, extensions to constant temperature and pressure simulations were implemented, as well as a parallel version of the integrator. The resulting MTS/PME algorithm for Newtonian and Langevin dynamics can be sketched as follows:

#### MTS/PME Algorithm

$$\begin{aligned} X_r^0 &\equiv X \\ F_{\text{slow}} &\equiv -\nabla E_{\text{slow}}(X_r) \\ P_i &= 0 \\ \text{For } j &= 1 \text{ to } k_2 \\ X_r &\equiv X_r^j \leftarrow X + \frac{\Delta t_m}{2} V \\ F_{\text{med}} &= -\nabla E_{\text{med}}(X_r) \\ F &\leftarrow F_{\text{med}} + F_{\text{slow}} \\ \text{For } i &= 1 \text{ to } k_1 \\ X &\leftarrow X + \frac{\Delta \tau}{2} V; \quad \text{SHAKE}\left(X, V, \frac{\Delta \tau}{2}\right); \\ &P_i = P_i + \text{get } P(X, V) \\ V &\leftarrow V(1 - \gamma \Delta \tau) + \mathbf{M}^{-1} \Delta \tau (F + F_{\text{fast}}(X) + R) \\ X &\leftarrow X + \frac{\Delta \tau}{2} V; \quad \text{SHAKE}\left(X, V, \frac{\Delta \tau}{2}\right) \\ \text{End} \\ \text{End} \\ P_i &= P_i / (k_1 k_2) \\ \text{scalX}(X, P_i, P_0, k_1 k_2 \Delta \tau) \end{aligned} \quad (9)$$

For Newtonian dynamics,  $R$  and  $\gamma$  are zero. Note here the similarity to the LN algorithm (see above) and the added SHAKE steps after each coordinate update. In addition, various MD ensembles were added to treat constant pressure and temperature ensembles. Besides the microcanonical ensemble (constant energy and volume, NVE), other ensembles that can be mimicked by the MTS/PME approach implemented in AMBER<sup>27</sup> are canonical (constant temperature and volume, NVT) and isothermal-isobaric (constant temperature and pressure, NPT). The implementations involve a weak coupling barostat for constant  $P$  and weak coupling thermostat for constant  $T$ , respectively, proposed by Berendsen and coworkers (see ref. 2 for a detailed discussion). In the algorithm sketched above, Cartesian positions were scaled to accommodate for constant pressure.

## Results and Discussion

### Biomolecular Systems

The two systems on which we examine the performance of various MTS/PME protocols are AMBER’s standard benchmark system, the dihydrofolate reductase (DHFR) solvated protein, which has a total of 22,930 atoms, and our pol  $\beta$ /DNA model<sup>31</sup> (Fig. 2). The latter involves the protein complexed to the primer/template DNA for a total of 40,673 atoms (11,399 bulk waters, 42  $\text{Na}^+$  ions, and 20  $\text{Cl}^-$  ions). All computations are performed on SGI Origin 2000/3000 computers with 8 300-MHz R12000 processors. Before the detailed algorithmic testing reported here, we have verified that the migration of the pol  $\beta$ /DNA model from CHARMM to AMBER has been successful (see Fig. 3A–C and corresponding caption).

### Accuracy: Comparison with Single Time Step

We now compare the accuracy of several MTS/PME protocols by examining the average of different energy components after running dynamics trajectories relative to the single-time step (STS) leapfrog Verlet integrator with  $\Delta t = 0.5$  as a reference. Figure 4 compares performance of the different Newtonian and Langevin MTS protocols as well as the STS scheme at  $\Delta t = 2$  fs over 400 ps relative to STS at  $\Delta t = 1$  fs.

We observe that in all cases relative errors are less than 2.5%, with smaller values for Newtonian protocols (relative to Langevin dynamics), as expected.

### Stability Limits and the Numerical PME Error

#### Determination of Stability Limit

We next examine the stability limits of our proposed MTS/PME algorithm. All calculations are performed on trajectories of length 400 ps to ensure that energy is well conserved. MTS/PME tests based on short trajectories of several picoseconds<sup>32</sup> can be misleading in detecting instabilities. Various MTS/PME protocols are considered in Figure 5, including those combinations near the stability limit (e.g., Newtonian protocol of 2/4/8 fs, Langevin protocol of 1/3/15 fs,  $\gamma = 5 \text{ ps}^{-1}$ ). All experiments

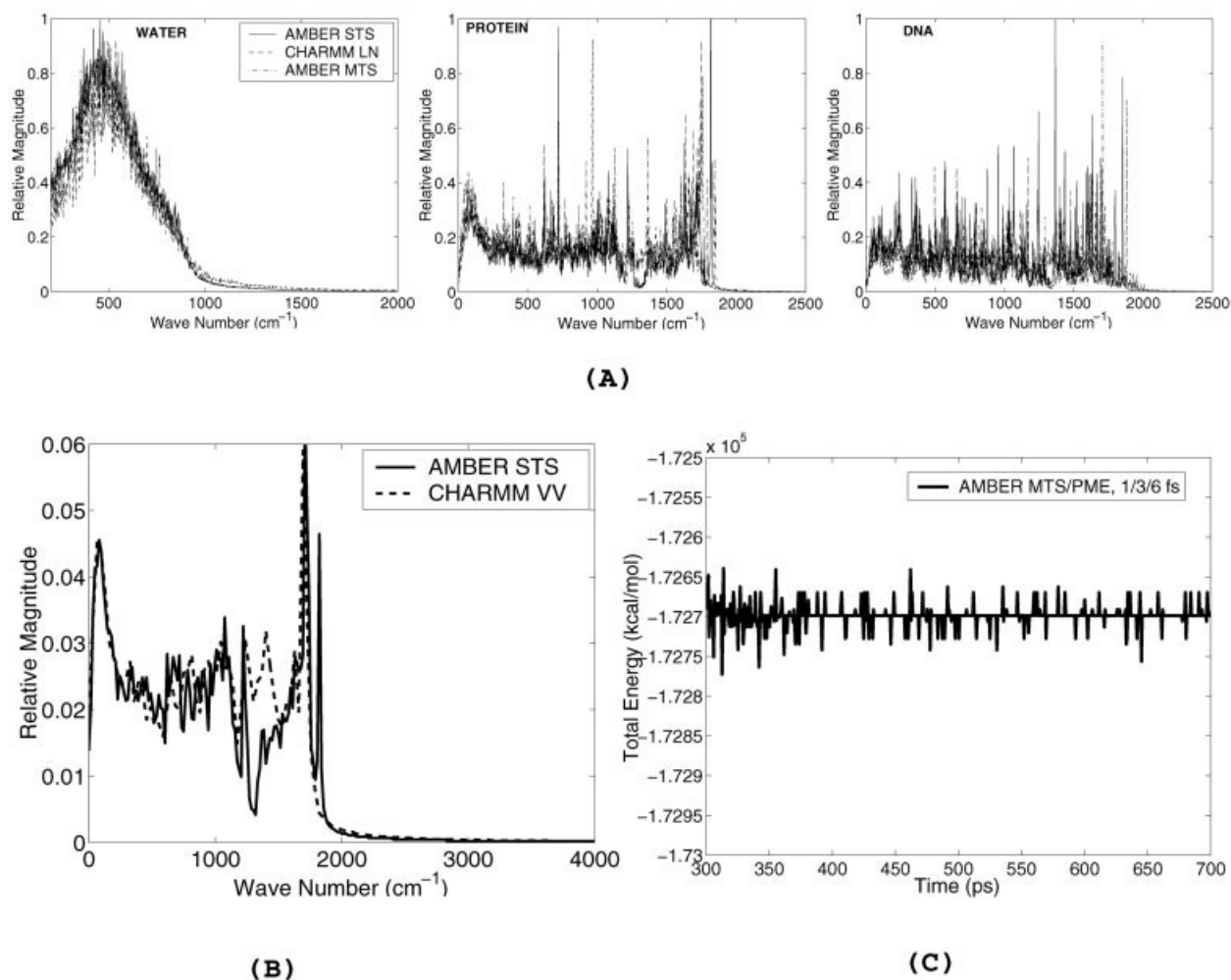


**Figure 3.** Tests on the polymerase  $\beta$  system. (A) Spectral density analysis for the water (left), protein (middle), and DNA (right) atoms of the pol  $\beta$ /DNA complex over a 12-ps trajectory. Spectral densities are compared from the LN algorithm in CHARMM (1/2/150 fs,  $\gamma = 10 \text{ ps}^{-1}$ ), single time step leapfrog Verlet integrator in AMBER (1 fs), and our MTS/PME method in AMBER (1/2/4 fs). Velocities of solute atoms are recorded every 2 fs. The overall similar trend in the spectra indicates successful migration from CHARMM to AMBER. (B) Spectral density analysis for the protein of the pol  $\beta$ /DNA complex over a 2-ps trajectory. The velocity Verlet in CHARMM and single time step leapfrog Verlet integrator in AMBER, both with a 1-fs time step, are compared. Velocities of solute atoms are recorded every 2 fs. Stretching frequencies are absent due to the application of SHAKE (constrained dynamics) on all bonds involving hydrogen. By comparing the spectra of two STS Newtonian schemes, successful migration from CHARMM to AMBER is further validated. (C) Energy conservation for pol  $\beta$ /DNA after 400 ps and equilibration, using MTS/PME protocol of 1/3/6 fs. Strict conservation of energy is achieved with the aforementioned protocol that represents a reliable conservative choice for the AMBER integrator.

reported involve constant energy simulations so as not to introduce additional complications (e.g., Berendsen thermostat, see ref. 2). In Table 1, two assessors commonly used for energy conservation,<sup>27</sup> namely the relative energy drift rate  $\kappa$  and the relative energy error  $\eta$ , are reported for these protocols. The drift rate  $\kappa$  in the least square sense (denoted by  $\doteq$ ) is defined as follows:

$$\frac{E_{\text{tot}}^i}{E_{\text{tot}}^0} \doteq \frac{\kappa}{t_u} t_i + b_0, \quad (10)$$

where  $t_i = i\Delta t$  at step  $i$ ,  $b_0$  is a parameter, and  $t_u$  is the preferred time unit to make  $\kappa$  unitless. The energy error is measured from the expression

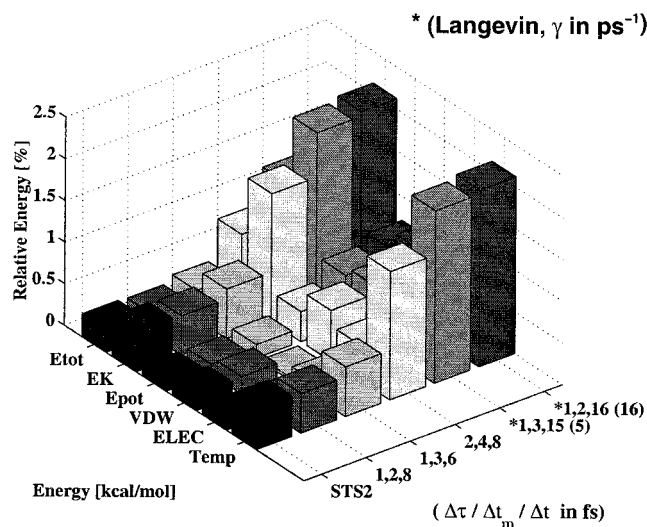


**Figure 4.** The deviation of energy components relative to the reference trajectory (single time step leapfrog Verlet Newtonian integration with  $\Delta t = 1.0$ ) for various MTS/PME protocols as indicated by triplets  $\Delta\tau/\Delta t_m/\Delta t$  fs ( $\gamma$  in  $\text{ps}^{-1}$ ) and the single time step leapfrog Verlet protocol at  $\Delta t = 2.0$  performed on the dihydrofolate reductase (DHFR) protein. All simulations are 400 ps in length.

$$\eta = \frac{1}{N_T} \sum_{i=1}^{N_T} \left| \frac{E_{\text{tot}}^i - E_{\text{tot}}^0}{E_{\text{tot}}^0} \right|, \quad (11)$$

where  $E_{\text{tot}}^i$  is the total energy at step  $i$ ,  $E_{\text{tot}}^0$  is the initial energy, and  $N_T$  is the total number of sampling points.

For the energy drift  $\kappa$ , a small  $\log_{10}\kappa$  value (low energy drift rate) is a good indicator of energy conservation. For the energy error  $\eta$ , a value of  $\log_{10}\eta < -2.5$  is considered acceptable in

**Table 1.** Energy Conservation Assessors for the Various Protocols Examined in Figure 5.

Protocol	$\log_{10}\eta$	$\log_{10}\kappa$
MTS 1/3/6 fs	-3.69	-6.35
MTS 2/4/8 fs	-2.95	-4.96
MTS 1/3/15 fs: Langevin, $\gamma = 5 \text{ ps}^{-1}$	-2.66	-6.31
MTS 1/2/16 fs: Langevin, $\gamma = 16 \text{ ps}^{-1}$	-2.67	-6.23
STS 2.0 fs	-4.18	-6.25
STS 1.0 fs	-4.10	-6.10

MTS: multiple time steps; STS: single time step leapfrog Verlet.

terms of numerical accuracy.<sup>37</sup> We observe in Table 1 that all protocols examined are acceptable in terms of the energy conservation assessors. They all exhibit small  $\log_{10}\kappa$  values and  $\log_{20}\eta$  values that are less than  $-2.5$ . For the MTS/PME Newtonian protocol of 2/4/8 fs and the Langevin protocol 1/3/15 fs with  $\gamma = 5 \text{ ps}^{-1}$ ,  $\log_{10}\eta$  approaches  $-2.5$  (threshold value). Indeed, for protocols with a larger outer time step than 8 fs (Newtonian), or 16 fs (Langevin), we find in Table 3 that  $\log_{10}\eta > -2.5$  and energy is no longer preserved.

#### A PME Source for Instabilities

The stability limits noted above—an outer time step of 8 fs in Newtonian protocols and 16 fs in Langevin protocols—can usually be detected only in simulations of length 400 ps or longer. A source of this instability not emphasized previously is the intramolecular cancellation error.<sup>33</sup> The need for a correction term arises because some near-neighbor nonbonded interactions are omitted from the Coulomb potential to avoid double counting these interactions in other terms of the potential. In practice, these excluded terms are subtracted from the Coulomb potential as evaluated by

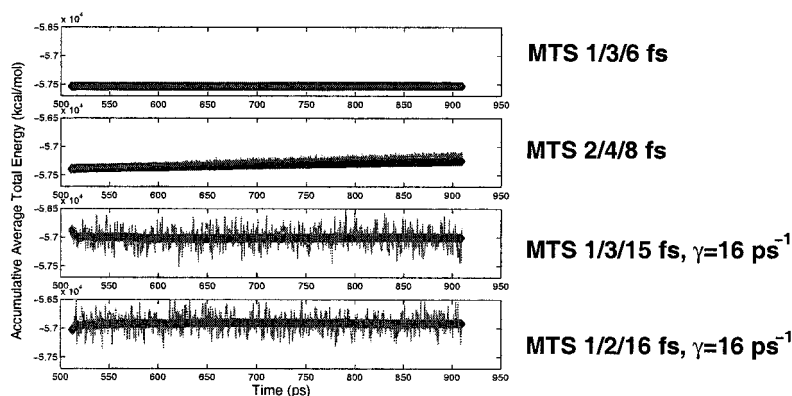


**Figure 5.** Energy conservation of various different protocols of the MTS/PME algorithm developed, performed on the dihydrofolate reductase (DHFR) protein for 400 ps. Evolution of total energy and accumulative average (thick line) is shown for each protocol. For references, the mean energies for the four protocols bottom to top are  $-56,917 \pm 159$ ,  $-56,942 \pm 153$ ,  $-57,253 \pm 75$  and  $-57,527 \pm 15$  kcal/mol, respectively.

PME. While in the direct-space sum, these excluded Coulombic interactions are simply omitted, in the reciprocal-space term, they are calculated only to a finite degree of accuracy due to the cutoff in the reciprocal-space grid; thus, the subtraction of the excluded terms does not exactly cancel the implicitly-contained analog (in the reciprocal-space summation). This cancellation error varies in time and introduces artificial frequencies to the governing dynamics motion. Unfortunately, we find that this numerical PME error cannot be easily eliminated by refining the PME parameters (grid resolution and/or order of interpolating polynomial).

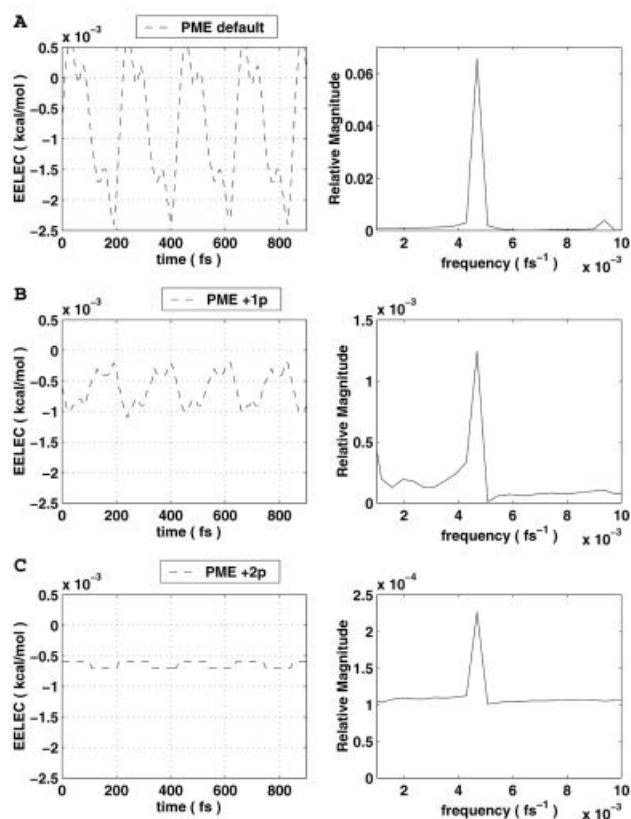
Procacci et al.<sup>33</sup> have devised a simple water system to examine the cancellation error for a single water molecule in a cubic box with side length of 64 Å, in which the total electrostatic energy corresponds exactly to the intramolecular cancellation error. In Qian and Schlick,<sup>27</sup> this error was further examined in AMBER using a single water molecule system.

Figure 6A (which uses default parameters of PME in AMBER) shows the magnitude of the cancellation error and its associated frequencies. The two characteristic periods on the order of 110 and 200 fs (inverse of the frequencies captured) impose an upper bound on the outer time step of 35 fs for linear stability (period over  $\pi$ )<sup>27,43</sup> and 25 fs to avoid fourth-order resonance (period over  $\sqrt{2}\pi$ ).<sup>27,41</sup>

#### Attempts to Suppress PME Error Source

To rule out other sources of errors, we have attempted to suppress this error by refining the PME parameters. It is possible that high-accuracy PME parameters might reduce the size of such cancellation errors and consequently dampen the instabilities from the integration. Specifically, we have systematically refined key PME parameters (1) *the direct-space grid*—by decreasing the tolerance of the direct sum part,<sup>29</sup> that by default in AMBER 6.0 is  $\epsilon_{\text{dir}} = 10^{-5}$ ; (2) *the reciprocal-space grid*—by refining the size of the charge grid upon which the reciprocal sums are interpolated, a grid that by default for the water system is  $64 \times 64 \times 64 \text{ \AA}^3$  (i.e., a refinement by a factor of 2 corresponds to  $128 \times 128 \times 128 \text{ \AA}^3$  for the water system); and (3) *the order of the B-spline interpolation polynomial* commonly used with the PME—by increasing the AMBER 6.0 default value of 4. Double-precision calculations are used throughout.

Although refining the direct-space grid does not affect the electrostatic energy in the single water molecule system (data not shown), we find that the combination of the other refinements (reciprocal-space grid resolution and B-spline order) appears to succeed in suppressing the cancellation error captured in the above system—see Figure 7C, which reveals no characteristic periods. However, a detailed examination of the systematic refinement steps in Figures 6, 7, and Table 2 reveals that the finite computer precision limits the result reported even though the error and its related frequencies remain unaltered. That is, although the oscillations around the mean error have been dampened, the mean value remains at approximately  $-0.0006 \text{ kcal/mol}$ , with the same characteristic periods present in the spectra, although at smaller relative magnitudes. Thus, it can be conjectured, based on the refinement steps reported in Table 2, that the combined effect of doubling the resolution of the reciprocal-space grid and increasing the order of



**Figure 6.** The intramolecular cancellation error (EELEC) for the default PME parameters in AMBER (A), PME refinement by increasing the order of the interpolating polynomial from 4 to 5 (B), PME refinement by increasing the order of the interpolating polynomial from 4 to 6 (C). Left: electrostatic energies of the single water molecule<sup>33</sup> calculated with a single time step of  $\Delta t = 0.5 \text{ fs}$  in AMBER 6.0 by leapfrog Verlet. Right: the spectral analysis of the autocorrelation function of electrostatic energy that reveal two characteristic periods on the order of 110 and 220 fs.

the interpolation polynomial by two terms still produces artifacts from the PME cancellation term.

We also remark that additional refinements performed in response to a referee’s suggestions, namely increasing the order of the B-spline interpolation polynomial from 4 to 12 and trying force-interpolated PME, have not succeeded in decreasing the lowest PME cancellation error that is reported in Table 2 (data not shown).

The CPU times associated with these refinements indicate that increasing the resolution of the reciprocal-space grid in the single water molecule system is costly (Table 2), but this example is not representative since a direct-space term is absent in the single water molecule.<sup>33</sup> In general, the direct-space term is the dominant part of the calculation; thus, for example, a refinement of the reciprocal-space resolution by a factor of two in the DHFR system yields an increase of the CPU times by no more than 35%, see Table 3. The change in CPU time when increasing the order of the interpolating polynomial is insignificant (Table 2); the slight decrease in the water system does not occur for larger systems.

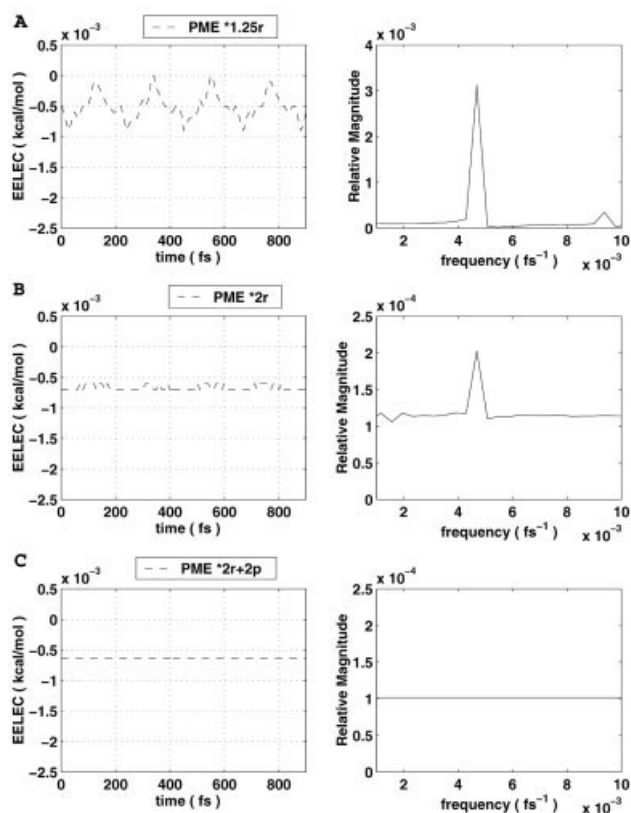


**Figure 7.** The intramolecular cancellation error (ELEC) for increasing the resolution of the reciprocal-space grid in AMBER's PME by a factor of 1.125 from the default value of a charge grid of  $64 \times 64 \times 64 \text{ \AA}^3$  (A), a factor of 2.0 (B), and a combination of a factor of 2.0 and an increase in the order of the interpolating polynomial from 4 to 6 (C). Left: electrostatic energies of the single water molecule<sup>33</sup> calculated with a single time step of  $\Delta t = 0.5$  in AMBER 6.0 by leapfrog Verlet. Right: the spectral analysis of the autocorrelation function of electrostatic energy.

We have also checked whether any suppression of cancellation error can be achieved for large systems the size of polymerase  $\beta$ /DNA (as introduced earlier). The same refinements of PME parameters (namely, the increase in the reciprocal-space grid resolution and the increase in the order of the interpolation polynomial) on the DHFR benchmark are examined in Table 3. We see that high-accuracy PME runs fail to suppress the cancellation error in larger systems, and the same stability limits mentioned above remain.

We have also experimented with subtraction of the intramolecular excluded correction term from the switched direct-space rather than the switched reciprocal-space term. Such a comparison has been performed,<sup>46</sup> and only a slight difference was noticed. Conceptually, the advantage of this subtraction in direct-space rather than reciprocal-space might be that the correction is accounted for more often, because the direct-space is assigned to the medium class and is propagated with smaller time steps. However, because the force is fluctuating more often, instabilities may also develop.

Additional tests (not reported in tables) reveal that the time step stability limits remain essentially the same whether the correction is done in the medium class or in the slow class. The reported energy drifts in Table 3 indicate that the subtraction of the excluded correction in direct-space, as in the case of reciprocal-space, results in significant energy drifts for both Newtonian and Langevin protocols that are above the stability limits mentioned (i.e., 8 fs for Newtonian, 16 fs for Langevin). These findings strengthen our conclusion that the excluded error accumulates no matter where the subtraction of the intramolecular excluded correction term is performed.

### Speedup

An analytical estimate for the maximal MTS speedup can be derived as follows.<sup>27</sup> We assume that evaluating the slow forces requires  $C_m$  amount of work and that the nonbonded computation dominates in total CPU cost. For MTS with an outer time step  $\Delta t$ , the total CPU cost can therefore be estimated approximately by  $(k_2 + 1)C_m$ . For a STS protocol with time step  $\Delta\tau_0$ , the total CPU cost to cover a time interval  $\Delta t$  is  $C_m(\Delta t/\Delta\tau_0) = k_1 k_2 C_m(\Delta\tau/\Delta\tau_0)$ . Therefore, the limiting MTS speedup is given by the ratio of these two estimates, which is

$$\frac{k_1 k_2}{k_2 + 1} \left( \frac{\Delta\tau}{\Delta\tau_0} \right). \quad (12)$$

In Figure 8, experimental results for the DHFR protein benchmark and pol  $\beta$ /DNA complex are plotted along with the analytical estimate for various MTS/PME protocols. We observe that in practice, the analytical estimate is not an upper bound; namely, it is possible to perform better than this estimate with well-tuned protocols.<sup>27</sup> When deriving the estimates, it was assumed that the nonbonded pair list is the same size for both the STS reference integrator and the MTS/PME protocols. However, by tuning the parameters of the switch functions, we could decrease the direct-space cutoff from the default value used in AMBER (i.e., from 8 to 7  $\text{\AA}$ ) without a significant loss in accuracy. This reduces the nonbonded list maintenance time for the electrostatic force update and yields greater speedups compared to the analytical estimate. Table 4 reports the speedup factors, also plotted in Figure 8, for both DHFR and pol  $\beta$ /DNA.

### Parallelization

A parallel version of the proposed MTS/PME algorithm is available for use in AMBER 6.0. The scalability of the algorithm was tested on an SGI Origin 2000 and SGI Origin 3000 computers. Relative to the STS integrator, the MTS/PME protocol requires more communication because of additional Message Passing Interface (MPI) calls to accommodate the multiple time steps. In MTS/PME, the percentage of work spent on the nonbonded computations are the part originally designed to scale well on multiple processors, the scalability of MTS/PME schemes is poorer than for STS schemes. Table 5 shows this trend. By increasing the number of processors, less time is spent on nonbonded computations in MTS/PME relative to STS and therefore a deviation from linear scalability results.



**Table 2.** Electrostatic Energies and CPU Times for the Single Water System in High Accuracy PME Runs.

PME protocol	Mean elec energy (kcal/mol)	RMS of elec energy (kcal/mol)	CPU (5-ps trajectory) (seconds)
STS 0.5 fs: def	-0.0008	0.0009	4639
STS 0.5 fs: +1p	-0.0006	0.0003	4429
STS 0.5 fs: +2p	-0.0006	0.00004	3721
STS 0.5 fs: *1.25r	-0.0005	0.0002	11069
STS 0.5 fs: *1.5r	-0.0006	0.0001	18424
STS 0.5 fs: *2r	-0.0007	0.00002	43373
STS 0.5 fs: *2r + 2p	-0.0006	0.0000004	45489

def: default PME parameters; \*1.25, \*1.5, \*2r: factor of 1.25, 1.5, 2 greater resolution of the reciprocal-space grid (i.e., grid dimensions of  $80 \times 80 \times 80 \text{ \AA}^3$ ,  $96 \times 96 \times 96 \text{ \AA}^3$ , and  $128 \times 128 \times 128 \text{ \AA}^3$ , respectively); +1p, +2p: increase in the order of the interpolating polynomial from 4 (cubic spline) to 5 or 6.

Moreover, the nonbonded pairlist is accessed twice within a macrostep interval  $\Delta t$  (as the slow and medium forces are recalculated) to compute a subtracted switched correction term for each Coulombic force evaluation. These additional operations impair the scalability of MTS relative to STS integrators. Figure 9 shows the MTS/PME scalability with a 1/3/6 fs protocol, relative to STS, as applied to the solvated dihydrofolate reductase protein and polymerase  $\beta$ /DNA systems.

## Conclusions

The MTS/PME algorithm described here builds on features of the LN algorithm in CHARMM (i.e., position rather than velocity Verlet; Langevin dynamics to mask mild instabilities) and is tailored to PME by using switch functions. By tuning the smooth

switches, a balance can be reached such that near-field contributions are removed from the reciprocal term while far-field contributions are removed from the direct term. Applying the smooth switches to both Coulomb and Van der Waals force terms is also preferable to using cutoffs in modeling biomolecular systems.

The performance analyses on both the dihydrofolate reductase (DHFR) protein benchmark and the large polymerase  $\beta$ /DNA complex have demonstrated the accuracy, speedup, and stability characteristic of different protocols, but have also identified a fundamental limitation inherent to MTS/PME algorithms due to the numerical approximation in the PME<sup>27,30,33</sup> approach. Namely, the intramolecular cancellation term in PME methods contributes to make MTS algorithms unstable beyond relatively small time steps (e.g., 8 fs or less for Newtonian, 16 fs for Langevin dynamics) (see Figs. 6, 7 and Table 2 for these error illustrated on a simple water system).

**Table 3.** Energy Conservation Assessors and CPU Times for the Solvated DHFR Model in High Accuracy PME Runs.

Protocol	$\log_{10}\eta$	$\log_{10}\kappa$	CPU (1 ps trajectory) (seconds)
MTS 1/2/8 fs: def	-3.32	-5.34	883
MTS 1/2/8 fs: *2r	-3.57	-5.36	1183
MTS 1/2/8 fs: +2p	-3.37	-5.40	948
MTS 1/2/10 fs: def	-1.92	-3.92	849
MTS 1/2/10 fs: *2r	-1.92	-3.91	1078
MTS 1/2/10 fs: +2p	-1.92	-3.92	890
MTS 1/2/12 fs: def	-0.54	-1.14	808
MTS 1/2/12 fs: *2r + 2p	-0.83	-2.75	1060
MTS 1/2/12 fs: *2r + 2p (d)	-0.22	-2.21	1069
MTS 1/2/18 fs: Langevin, $\gamma = 16 \text{ ps}^{-1}$ , def	-1.92	-3.81	838
MTS 1/2/18 fs: Langevin, $\gamma = 16 \text{ ps}^{-1}$ , *2r + 2p (d)	-1.93	-4.22	1036

def: default PME parameters; \*1.25r, \*1.5r, \*2r: factor of 1.25, 1.5, 2 greater resolution of the reciprocal-space grid (i.e., grid dimensions of  $80 \times 80 \times 80 \text{ \AA}^3$ ,  $96 \times 96 \times 96 \text{ \AA}^3$ , and  $128 \times 128 \times 128 \text{ \AA}^3$ , respectively); +1p, +2p: increase in the order of the interpolating polynomial from 4 (cubic spline) to 5 or 6. The suffix (d) indicates subtraction of the excluded correction term from direct-space, rather than from reciprocal-space.

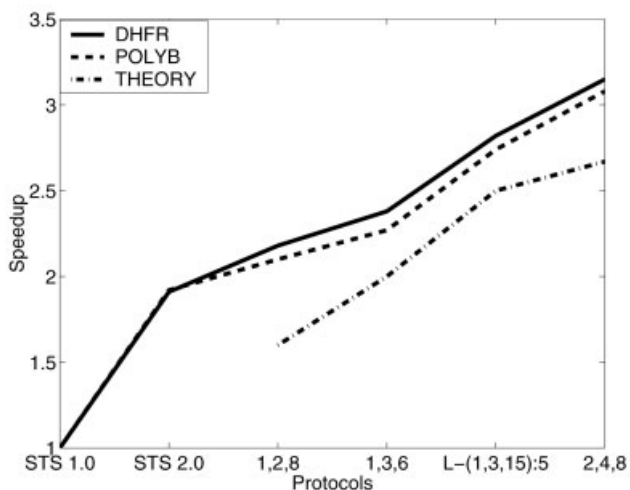


**Figure 8.** Speedup for various MTS/PME protocols, relative to the single time step integrator by leapfrog Verlet with  $\Delta t = 1.0$  fs. All simulations are 1 ps in length and use a single processor. Speedup factors are based on simulations performed on the SGI Origin 2000 with 8 300-MHz R12000 processors. The simulations were performed on the dihydrofolate reductase (DHFR) protein and polymerase  $\beta$ /DNA systems. Results of a theoretical estimate based on eq. (12) are also given for reference.

The intramolecular Coulomb interactions between certain pairs of atoms within the same molecule are excluded in the force field, and therefore should be subtracted from the Coulomb summation. The contribution from intramolecular Coulomb interactions is automatically included in the reciprocal space summation when using the PME methodology for the electrostatics. The subtraction of the excluded correction term, computed exactly, cannot precisely cancel the addition to the reciprocal-space Ewald summation that is computed approximately due to the cutoff in reciprocal space. The cancellation error that is produced as a consequence causes instabilities when the time step becomes larger. Table 4 illustrates the speedup limitations that are encountered, and Table 5 demonstrates the scalability problems associated with the incorporation of MTS into the PME.

In an earlier section (Tables 2, 3, Figs. 6, 7) we attempted to suppress the intramolecular cancellation error by increasing the

**Table 4.** Speedup for the Efficient MTS/PME Protocols and the Single Time Step Leapfrog Verlet Integrator with  $\Delta t = 2.0$  fs, Relative to the Single Time Step Leapfrog Verlet Integrator with  $\Delta t = 1.0$  fs for the DHFR and pol  $\beta$  Systems, as Calculated over 1 ps.

Protocol	DHFR	pol $\beta$
MTS 2/4/78 fs	3.15	3.08
MTS 1/3/15 fs: Langevin, $\gamma = 5 \text{ ps}^{-1}$	2.82	2.74
MTS 1/3/6 fs	2.38	2.27
MTS 1/2/8 fs	2.18	2.10
STS 2.0 fs	1.91	1.92

**Table 5.** Percentage of Time Spent in Nonbonded Computations.

Processors	STS (%)	MTS (%)	Ratio of MTS/STS
1	95.41	88.44	0.93
2	93.34	82.88	0.89
4	88.79	72.12	0.81
8	78.61	53.77	0.68

accuracy of the PME computation (i.e., refining the grid used in both the direct and reciprocal spaces and increasing the order of the interpolating polynomial). Indeed, for the small, constructed system of a single water molecule in which the cancellation error is the total energy,<sup>27,33</sup> it might appear that we can suppress the error by increasing the reciprocal-space grid by a factor of two and increasing the order of the B-spline interpolating polynomial from 4 to 6. However, this only reflects the suppression of the oscillations around the mean and not the presence of artificial periods, as discussed earlier. We have verified that performing these refinements on the polymerase  $\beta$ /DNA system (see Table 3) does not allow us to increase the outer time step beyond the limits mentioned above. Constructing a suitable correction potential to attempt a suppression of this instability, as suggested by Procacci et al.<sup>33</sup> for the single water molecule system, is an involved task for large biomolecular systems.

Based on these findings, we conclude that this contributor of instabilities in MTS/PME protocols—the intramolecular cancellation error—cannot easily be controlled in general. In systems the size of the polymerase  $\beta$ /DNA complex, the instabilities at large outer time steps do not disappear by attempting to suppress the cancellation error with high accuracy PME runs. Perhaps some augmentation to the PME formulations are possible,<sup>47</sup> but this

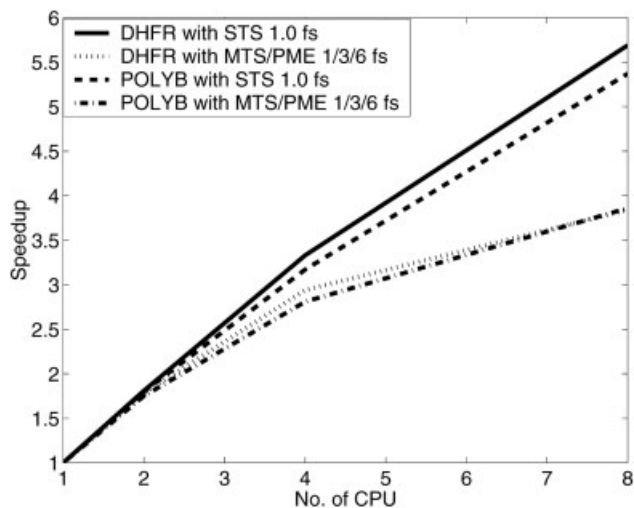


**Figure 9.** Parallel scalability of different STS by leapfrog Verlet and MTS (as described in the text) protocols, implemented in AMBER 6.0 and tested on an SGI Origin 3000 computer relative to a single processor. All simulations were performed for 1 ps. Speedup ratios exclude setup times.

remains to be tested. Artifacts from the periodic boundary conditions (e.g., references 48–51) may also be an issue that is difficult to address in practice. We thus suggest that the larger time steps needed to make MTS algorithms advantageous (e.g., references 25, 31, 32, 52–56) can be accomplished by methods other than the PME for fast electrostatics.

## Appendix

The Ewald summation consists of the following terms for the Coulomb potential,<sup>2</sup>

$$E_C = E_{\text{direct}} + E_{\text{reciprocal}} + E_{\text{cor,self}} + E_{\text{cor,ex}} + E_{\text{cor,\varepsilon}} \quad (13)$$

where

$$E_{\text{real}} = \frac{1}{2} \sum_{i,j=1}^N q_i q_j \sum_{\mathbf{n}} \frac{\text{erfc}(\beta |\mathbf{r}_{ij} + \mathbf{n}|)}{|\mathbf{r}_{ij} + \mathbf{n}|}; \quad (14)$$

$$E_{\text{recip.}} = \frac{1}{2\pi L^3} \sum_{|\mathbf{m}| \neq 0} \frac{\exp(-\pi^2 |\mathbf{m}|^2 / \beta^2)}{|\mathbf{m}|^2} G(\mathbf{m}) G(-\mathbf{m}),$$

$$G(\mathbf{m}) = \sum_{j=1}^N q_j \exp[2\pi i \mathbf{m} \cdot \mathbf{x}_j]; \quad (15)$$

$$E_{\text{cor,self}} = \frac{-\beta}{\sqrt{\pi}} \sum_{j=1}^N q_j^2; \quad (16)$$

$$E_{\text{cor,ex}} = -\frac{1}{2} \sum_{i,j \in \text{Ex.}} q_i q_j \frac{\text{erf}(\beta |\mathbf{r}_{ij}|)}{|\mathbf{r}_{ij}|}; \quad (17)$$

$$E_{\text{cor,\varepsilon}} = \frac{2\pi}{(1 + 2\varepsilon)L^3} \left| \sum_{j=1}^N q_j \mathbf{x}_j \right|^2. \quad (18)$$

Here,  $\beta$  is the Ewald constant,  $q_i$  is the partial charge on atom  $i$ , and  $\text{erfc}(x)$  is the complementary error function ( $\text{erfc}(x) = 2/\sqrt{\pi} \int_x^\infty \exp(-u^2) du$ ). For the reciprocal term we sum over Fourier modes where  $\mathbf{m} = 2\pi \mathbf{k}/L$ ,  $V = L^3$ ,  $m = |\mathbf{m}| = 2\pi |\mathbf{k}|/L$ , and  $\mathbf{k} = (k_x, k_y, k_z)$ ,  $k_x, k_y, k_z$  are integers, and  $L^3$  is the volume of the cubic domain. The non-Coulomb potentials in the system are:

$$E_{NC} = E_r + E_\theta + E_\tau + E_{LJ} + E_{Hb}, \quad (19)$$

where

$$E_r = \sum_{i,j \in S_B} S_{ij} (r_{ij} - \bar{r}_{ij})^2 \quad (20)$$

$$E_\theta = \sum_{i,j,k \in S_{BA}} K_{ijk} (\theta_{ijk} - \bar{\theta}_{ijk})^2 \quad (21)$$

$$E_\tau = \sum_{i,j,k,l \in S_{DA}} \sum_n \frac{V_{ijkl}}{2} (1 + \cos(n\pi_{ijkl})) \quad (22)$$

$$E_{LJ} = \sum_{i<j} 4\varepsilon_{ij} \left( \frac{\sigma_{ij}^{12}}{r_{ij}^{12}} - \frac{\sigma_{ij}^6}{r_{ij}^6} \right) + \frac{1}{E_{\text{scale}}^{1,4}} \sum_{i<j} 4\varepsilon_{ij} \left( \frac{\sigma_{ij}^{12}}{r_{ij}^{12}} - \frac{\sigma_{ij}^6}{r_{ij}^6} \right) \quad (23)$$

$$E_{Hb} = \sum_{i<j} \left( \frac{C_{ij}}{r_{ij}^{12}} - \frac{D_{ij}}{r_{ij}^{10}} \right). \quad (24)$$

Smooth switches are employed using the following switch function for the switch interval  $[r_0, r_1]$ ,

$$S(r, r_0, r_1) = \begin{cases} 1 & \text{if } r \leq r_0, \\ x^2(2x - 3) + 1 & \text{if } r_0 < r < r_1, \\ 0 & \text{if } r \geq r_1, \end{cases} \quad (25)$$

where  $x = (r - r_0)/(r_1 - r_0)$ .

## Acknowledgments

We thank Drs. Suse Broyde (Department of Biology, New York University), David A. Case (Department of Molecular Biology, The Scripps Research Institute), and Tom Darden (National Institutes of Environmental Health Sciences) for helpful comments.

## References

- Pearlman, D. A.; Case, D. A.; Caldwell, J. W.; Ross, W. S.; Cheatham, T. E., III; DeBolt, S.; Ferguson, D.; Seibel, G. L.; Kollman, P. A. *Comp Phys Commun* 1995, 91, 1.
- Schlick, T. *Molecular Modeling and Simulation: An Interdisciplinary Guide*. Springer-Verlag: New York, 2002. (<http://www.springer-ny.com/detail.tpl?isbn=038795404X>)
- Wang, W.; Donini, O.; Reyes, C. M.; Kollman, P. A. *Annu Rev Biophys Biomol Struct* 2001, 30, 211.
- Brooks, C. L., III; Karplus, M.; Pettitt, B. M. *Advances in Chemical Physics*; John Wiley & Sons: New York, 1988.
- McCammon, J. A.; Harvey, S. C. *Dynamics of Proteins and Nucleic Acids*; Cambridge University Press: Cambridge, MA, 1987.
- Beveridge, D. L.; Lavery, R., Editors. *Theoretical Biochemistry and Molecular Biophysics*; Adenine Press: Guilderland, NY, 1991.
- Schlick, T.; Skeel, R. D.; Brunger, A. T.; Kalé, L. V., Jr.; Hermans, J. J.; Schulten, K. *J Comp Phys* 1999, 151, 9.
- Schlick, T. *J Comput Phys* 1999, 151, 1 (Special Volume on Computational Biophysics).
- Schlick, T., Editor. *Computational Molecular Biophysics*; Academic Press: San Diego, CA, 1999; vol. 151.
- van Gunsteren, W. F.; Weiner, P. K., Eds. *Computer Simulation of Biomolecular Systems*; ESCOM: Leiden, The Netherlands, 1989; vol. 1.
- van Gunsteren, W. F.; Weiner, P. K.; Wilkinson, A. J., Eds. *Computer Simulation of Biomolecular Systems*; ESCOM: Leiden, The Netherlands, 1993; vol. 2.
- van Gunsteren, W. F.; Weiner, P. K.; Wilkinson, A. J., Eds. *Computer*

- Simulation of Biomolecular Systems; ESCOM: Leiden, The Netherlands, 1996; vol. 3.
13. Deuffhard, P.; Hermans, J.; Leimkuhler, B.; Mark, A. E.; Reich, S.; Skeel, R. D., Eds. Proceedings of the 2nd International Symposium on Algorithms for Macromolecular Modelling, Berlin, May 21–24, 1997; volume 4 of Lecture Notes in Computational Science and Engineering (Griebel, M.; Keyes, D. E.; Nieminen, R. M.; Roose, D.; Schlick, T., Series Eds.); Springer-Verlag: Berlin, 1999.
  14. Beveridge, D. L.; McConnell, K. J. *Curr Opin Struct Biol* 2000, 10, 182.
  15. Warshel, A.; Parson, W. W. Dynamics of biochemical and biophysical reactions: Insight from computer simulations. *Q Rev Biophys* 2001, 34, 563.
  16. Brooks, C. L., III. Viewing protein folding from many perspectives. *Proc Natl Acad Sci USA* 2002, 99, 1099.
  17. Chance, M. R.; Bresnick, A. R.; Burley, S. K.; Jiang, J.-S.; Lima, C. D.; Sali, A.; Almo, S. C.; Bonanno, J. B.; Buglino, J. A.; Boulton, S.; Chen, H.; Eswar, N.; He, G.; Huang, R.; Ilyin, V.; McMahan, L.; Pieper, U.; Ray, S.; Vidal, M.; Wang, L. K. *Protein Sci* 2002, 11, 723.
  18. Greengard, L.; Rokhlin, V. A fast algorithm for particle simulation. *J Comp Phys* 1987, 73, 325.
  19. Darden, T.; York, D. M.; Pedersen, L. G. *J Chem Phys* 1993, 98, 10089.
  20. Brandt, A. *Math Comput* 1977, 31, 333.
  21. Sandak, B. *J Comp Chem* 2001, 22, 717.
  22. Sagui, C.; Darden, T. *J Chem Phys* 2001, 114, 6578.
  23. Streett, W. B.; Tildesley, D. J.; Saville, G. *Mol Phys* 1978, 35, 639.
  24. Swindoll, R. D.; Haile, J. M. *J Chem Phys* 1984, 53, 289.
  25. Tuckerman, M. E.; Berne, B. J.; Martyna, G. J. *J Chem Phys* 1992, 97, 1990.
  26. Grubmüller, H.; Heller, H.; Windemuth, A.; Schulten, K. *Mol Sim* 1991, 6, 121.
  27. Qian, X.; Schlick, T. *J Chem Phys* 2002, 116, 5971.
  28. Cheatham, T. E., III; Miller, J. L.; Fox, T.; Darden, T. A.; Kollman, P. A. *J Am Chem Soc* 1995, 117, 4193.
  29. Essman, U.; Perera, L.; Berkowitz, M. L.; Darden, T.; Lee, H.; Pedersen, L. G. *J Chem Phys* 1995, 103, 8577.
  30. Batcho, P. F.; Case, D. A.; Schlick, T. *J Chem Phys* 2001, 115, 4003.
  31. Yang, L.; Beard, W. A.; Wilson, S. H.; Broyde, S.; Schlick, T. *J Mol Biol* 2002, 317, 651.
  32. Zhou, R.; Harder, E.; Xu, H.; Berne, B. J. *J Chem Phys* 2001, 115, 2348.
  33. Procacci, P.; Marchi, M.; Martyna, G. J. *J Chem Phys* 1998, 108, 8799.
  34. Stuart, S. J.; Zhou, R.; Berne, B. J. *J Chem Phys* 1996, 105, 1426.
  35. Schlick, T.; Yang, L. In Brandt, A.; Bernholc, J.; Binder, K., Eds.; *Multiscale Computational Methods in Chemistry and Physics*, NATO Science Series: Series III Computer and Systems Sciences; IOS Press: Amsterdam, 2001; p 293, vol. 177.
  36. Skeel, R. D.; Tezcan, I.; Hardy, D. J. *J Comp Chem* 2002, 23, 673.
  37. Figueirido, F.; Levy, R.; Zhou, R.; Berne, B. *J Chem Phys* 1997, 106, 9835.
  38. Duan, Z.-H.; Krasny, R. *J Comp Chem* 2001, 22, 184.
  39. Verlet, L. *Phys Rev* 1967, 159, 98.
  40. Störmer, C. *Arch Sci Phys Nat* 1997, 24, 5, 113, 221.
  41. Sandu, A.; Schlick, T. *J Comp Phys* 1999, 151, 74.
  42. Barth, E.; Schlick, T. *J Chem Phys* 1998, 109, 1633.
  43. Barth, E.; Schlick, T. *J Chem Phys* 1998, 109, 1617.
  44. Batcho, P. F.; Schlick, T. *J Chem Phys* 2001, 115, 4019.
  45. Press, W. H.; Teukolsky, S. A.; Vetterling, W. T.; Flannery, B. P. *Numerical Recipes in C*; Cambridge University Press: Cambridge, 1992. (<http://www.nr.com/>)
  46. Komeiji, Y. *J Mol Struct (Theochem)* 2000, 530, 237.
  47. Batcho, P. F.; Schlick, T. *J Chem Phys* 2001, 115, 8312.
  48. Smith, S. B.; Cui, Y.; Bustamante, C. *Science* 1996, 271, 795.
  49. Hünenberger, P. H.; McCammon, J. A. *J Chem Phys* 1999, 110, 1856.
  50. Hünenberger, P. H.; McCammon, J. A. *Biophys Chem* 1999, 78, 69.
  51. Hansson, T.; Oostenbrink, C.; van Gunsteren, W. F. *Curr Opin Struct Biol* 2002, 12, 190.
  52. Kalé, L.; Skeel, R.; Bhandarkar, M.; Brunner, R.; Gursoy, A.; Krawetz, N.; Phillips, J.; Shinozaki, A.; Varadarajan, K.; Schulten, K. *J Comput Phys* 1999, 151, 283.
  53. Chun, H. M.; Padilla, C. E.; Chin, D. N.; Watanabe, M.; Karlov, V. I.; Alper, H. A.; Soosar, K.; Blair, K. B.; Becker, O.; Caves, L. S. D.; Nagle, R.; Haney, D. N.; Farmer, B. L. *J Comp Chem* 2000, 21, 159.
  54. Watanabe, M.; Karplus, M. *J Phys Chem* 1995, 99, 5680.
  55. Izaguirre, J. A.; Reich, S.; Skeel, R. D. *J Chem Phys* 1999, 110, 9853.
  56. Schlick, T. *Structure* 2001, 9, R45.